Structural basis of the Sir1–origin recognition complex interaction in transcriptional silencing

Zhonggang Hou, Douglas A. Bernstein, Catherine A. Fox[†‡], and James L. Keck[†‡]

Department of Biomolecular Chemistry, University of Wisconsin Medical School, Medical Sciences Center, 1300 University Avenue, Madison, WI 53706-1532

Communicated by James E. Dahlberg, University of Wisconsin Medical School, Madison, WI, April 28, 2005 (received for review March 15, 2005)

The Sir1 protein plays a key role in establishing a silent chromatin structure at the cryptic mating-type loci *HMR* and *HML* in *Saccharomyces cerevisiae* by interacting with the bromo-adjacent homology (BAH) domain of the Orc1p subunit of the origin recognition complex (ORC). Here, we present the high-resolution crystal structures of the ORC interaction region (OIR) of Sir1p and that of the complex formed between the OIR and BAH domains. Amino acids within the OIR previously shown to be required for a Sir1p/ORC interaction are presented on a conserved, convex surface that forms a complementary interface with a concave region of the Orc1 BAH domain that is critical for transcriptional silencing. The OIR/BAH interaction surface comprises a network of hydrophobic and polar/ionic interactions between discrete structural modules in each protein and involves several residues that were not implicated in previous studies. These data provide important structural insights into a protein–protein interaction critical for the formation of a specialized chromatin domain within eukaryotic chromosomes.

chromatin | silencers | yeast | chromosomes | replication

Assembly of eukaryotic genomes into chromatin, chromosomal DNA and its bound proteins, has a profound impact on every aspect of chromosome biology (1, 2). Within an organism, chromatin structures vary significantly with genome position to create heterogeneity that is critical for spatial regulation of chromosome function (3). The mechanisms that regulate formation of chromatin structures to discrete positions of the eukaryotic genome define fundamental strategies critical to all eukaryotic cells.

Transcriptional silencing of the cryptic mating-type loci, *HMR* and *HML*, in the yeast *Saccharomyces cerevisiae* serves as a paradigm for understanding mechanisms that control the formation of specialized chromatin domains (4). The assembly of silent chromatin is targeted and confined specifically to *HMR* and *HML* by the action of DNA sequences called silencers present at these loci. Silencers are bound by sequence-specific DNA-binding proteins (silencer-binding proteins) that in turn recruit a set of four silent information regulator (Sir) proteins that cause transcriptionally repressive modification of the nucleosome array comprising *HMR* and *HML*.

Silencer-binding proteins include the origin recognition complex (ORC), a conserved six-subunit heteromeric protein complex that binds replication origins and is essential for the initiation of DNA replication in all eukaryotes (5). Analyses of *HMR*-E, a silencer that is necessary and sufficient to target silent chromatin to *HMR*, has established that the primary role for ORC in silencing is to recruit Sir1p to the silencer through direct protein–protein interactions between the Orc1p subunit of ORC and Sir1p (6–11). ORC-bound Sir1p nucleates and/or stabilizes a silent chromatin domain through direct protein–protein interactions with other Sir proteins, in particular Sir4p (7, 11). Thus, formation of the Sir1p/ORC interaction is a critical step in establishing a repressive chromatin structure at *HMR* (12).

Molecular and genetic analyses have shown that the Sir1p/ORC interaction occurs through direct contacts between discrete domains within each protein. In ORC, the key interaction domain is the N-terminal bromo-adjacent homology (BAH) domain of Orc1p (10, 13). BAH domains are conserved in Orc1 homologs across species (14) and are found in several other chromatin-associated proteins (15, 16), suggesting that BAH domains play broad roles in regulating the structure and function of chromosomes. The crystal structure of the *S. cerevisiae* Orc1p-BAH domain has been determined and serves as the guide for modeling other BAH domains (10). The domain of Sir1p required for the Sir1p/ORC interaction, the ORC interaction region (OIR) (11), is the only molecularly defined BAH-domain-binding partner and thus is key for understanding the function and mechanisms of BAH-domain-containing proteins and their binding partners in regulating chromatin structure.

In this report, we define the structural basis for the Sir1p/ORC interaction by defining the high-resolution crystal structures of the isolated Sir1p-OIR and the OIR bound to the Orc1-BAH domain from *S. cerevisiae*. The OIR forms a fold that includes a conserved structural subdomain containing residues previously identified as important for interacting with ORC. In the OIR/BAH complex, this conserved surface is enveloped by a region of the Orc1-BAH that has striking chemical and structural complementarities to Sir1p-OIR. The interface includes regions from both domains that have been predicted to be important for their interaction but also identifies several additional interaction surfaces between the domains. Together with the previously determined Orc1-BAH domain structure (10), these insights offer an atomic-level view of the complex cellular processes essential for formation of specialized chromatin domains.

Materials and Methods

Expression and Purification of Wild-Type and Mutant Forms of Sir1p-OIR. The sequence of *S. cerevisiae SIR1* that encodes the Sir1p-OIR (amino acids 480–611 of Sir1p) was amplified by PCR and introduced into the NheI site of pET28b (Novagen), creating pET28b-$(His)_6$-Sir1p-OIR for expression of $(His)_6$-OIR. A mutation that replaces the Cys-593 codon with an Ala codon was made in pET28b-$(His)_6$-Sir1p-OIR by using QuikChange mutagenesis (Stratagene), creating pET28b-$(His)_6$-Sir1p-OIR*. *E. coli* strain BL21 (DE3) transformed with pET28b-$(His)_6$-Sir1p-OIR* was grown in LB medium supplemented with 100 μg/ml kanamycin at 37°C. At an OD_{600} of ≈0.5, $(His)_6$-OIR* expression was induced with 1 mM isopropyl β-D-thiogalactopyranoside for 3 h. Cells were harvested by centrifugation, frozen at −80°C, resuspended at 4°C in lysis buffer (50 mM Hepes, pH 6.5/500 mM NaCl/10% glycerol/20 mM imidazole), supplemented with protease inhibitors and DNaseI, and lysed by

Abbreviations: BAH, bromo-adjacent homology; ORC, origin recognition complex; OIR, ORC interaction region; SRD, silencer-recognition defective.

Data deposition: Model coordinates and structure factors have been deposited in the Protein Data Bank, www.pdb.org (PDB ID codes 1Z1A and 1ZHI).

[†]C.A.F. and J.L.K contributed equally to this work.

[‡]To whom correspondence may be addressed. E-mail: cfox@wisc.edu or jlkeck@wisc.edu.

© 2005 by The National Academy of Sciences of the USA

BIOCHEMISTRY

Table 1. Data collection, refinement statistics, and phasing

	OIR*			
	Se peak	Se inflection	Remote	OIR*/BAH
Data collection				
Wavelength, Å	0.9793	0.9795	0.9688	0.9793
Resolution range, Å	25–2.5 (2.6–2.5)	25–2.5 (2.6–2.5)	25–2.5 (2.6–2.5)	62–2.7 (2.85–2.7)
Completeness, %	98.3 (91.8)	97.7 (87.6)	97.2 (84.9)	98.7 (98.7)
Total observations	127,815	121,606	61,314	153,162
Unique reflections	11,994	11,950	11,801	14,005
$\langle I/\sigma I\rangle$	40.0 (3.4)	36.8 (2.6)	25.9 (2.1)	13.6 (4.4)
R_{sym},† %	6.1 (33.1)	4.6 (36.5)	4.9 (32.0)	11.8 (51.7)
Phasing (OIR*)				
Figure of merit	0.342; 0.756 after solvent flattening			
Refinement				
Resolution, Å		20–2.5		18–2.7
R_{work}/R_{free}‡ %		23.8/27.4		23.1/29.3
rms deviations				
Bonds, Å		0.011		0.011
Angles, °		1.012		1.020
Ramachandran plot, %				
Most favored		92.8		86.5
Allowed		7.2		12.5
Generously allowed		0.0		0.3
Disallowed		0.0		0.7

Values in parentheses represent data ranging 2.6–2.5 Å for OIR* and 2.85–2.7 for OIR*/BAH.
†$R_{sym} = \Sigma\Sigma j|Ij - \langle I\rangle|\Sigma Ij$, where Ij is the intensity measurement for reflection j and $\langle I\rangle$ is the mean intensity for multiply recorded reflections.
‡$R_{work}/R_{free} = \Sigma||F_{obs}| - |F_{calc}||/|F_{obs}|$, where the working and free R factors are calculated by using the working and free reflection sets, respectively. The free R reflections (5% of the total) were held aside throughout refinement.

French press. The extract, after clearing by centrifugation (38,000 × *g* for 15 min), was incubated with Ni-NTA beads (Novagen) for 1 h at 4°C and packed into a column (settled bed volume of 2 ml). The resin was washed with 10 column volumes of lysis buffer, and $(His)_6$-OIR* was eluted with elution buffer (lysis buffer with 500 mM imidazole). Eluted $(His)_6$-OIR* was buffer-exchanged into lysis buffer with 50 units of thrombin to remove the $(His)_6$ tag. The cleaved protein was then passed over a Ni-NTA column a second time, and unbound protein was dialyzed into 50 mM Hepes, pH 6.5/50 mM NaCl/10% glycerol and loaded onto a SP-Sepharose column. The cleaved protein was then eluted with a linear (0.05 M to 0.50 M) NaCl gradient. Fractions containing OIR* were pooled, concentrated, and further purified on a Sephacryl S-100 column (Amersham Biosciences) equilibrated in S-100 buffer (50 mM Hepes, pH 6.5/500 mM NaCl/10% glycerol).

Expression and Purification of the Orc1p-BAH Domain. The coding region for *S. cerevisiae* Orc1p amino acids 1–219 was amplified by PCR and cloned into pET28b by using the NheI site. The expression and purification protocols were essentially the same as those used for the OIR*.

Crystallization and Structure Determinations of Sir1p-OIR*. Purified OIR* was dialyzed into 10 mM Hepes, pH 6.5/50 mM NaCl before crystallization. Crystals were grown by hanging drop vapor diffusion by mixing 1 μl of protein (≈9 mg/ml) with 1 μl of well solution (0.1 M sodium acetate pH 5.5/25–30% polyethelene glycol 400) and incubating at room temperature for several days. Selenomethionine-incorporated OIR* was purified similarly to the native protein except that 1 mM tri(2-carboxyethyl) phosphine hydrochloride was present in all buffers, and the S-100 gel-filtration step was omitted. Crystallization conditions for the selenomethionine-substituted protein were modified to 0.1 M sodium acetate pH 5.5/28–30% polyethelene glycol 400/4–8% glycerol/1 mM tri(2-carboxyethyl) phosphine hydrochloride, and drops were streak-seeded with native crystals. Crystals of selenomethionine-incorporated OIR* were frozen directly from drops in liquid nitrogen for data collection. Crystals diffracted to 2.5-Å resolution with $P3_221$ symmetry and unit cell dimensions of $a = b = 60.93$ Å and $c = 159.26$ Å, consistent with two molecules per asymmetric unit (17). Noncrystallographic symmetry restraints were not used in the structure determination to allow independent refinement of each OIR* domain.

The structure of selenomethionine-incorporated OIR* was solved by using multiwavelength anomalous dispersion phasing (Table 1). Data were indexed and scaled with HKL2000 (18), and selenium sites were identified by using SOLVE (19) and further refined with MLPHARE (20). Solvent flattening with DM (21) resulted in interpretable experimental electron density maps for manual model building with the program O (22). Rounds of refinement with REFMAC5/ARP (23, 24) and manual rebuilding improved the model.

Crystallization and Structure Determinations of the Sir1p-OIR*/Orc1p-BAH Complex. Separately purified pools of OIR* and Orc1p-BAH domain were mixed at a molar ratio of 1.1:1, incubated on ice for 30 min, and then applied to a Sephacryl S-100 gel filtration column (Amersham Biosciences) equilibrated in S-100 buffer (50 mM Hepes, pH 6.5/500 mM NaCl/10% glycerol). Protein fractions containing the OIR*/Orc1p-BAH complex were pooled, concentrated to 10 mg/ml, and dialyzed into 10 mM Hepes, pH 6.5/50 mM NaCl before crystallization. Crystals were grown by hanging drop vapor diffusion by mixing 1 μl of protein with 1 μl of well solution [0.1 M Tris, pH 7.5/0.1 M NaCl/1.3–1.5 M $(NH_4)_2SO_4$] and incubating at room temperature for several days. Diffraction quality crystals were obtained by streak-seeding drops preequilibrated against the same well solution and were transferred to cryoprotectant solution [0.1 M Tris, pH 7.5/0.1 M NaCl/1.8 M $(NH_4)_2SO_4$/25% glycerol] and then frozen in liquid nitrogen for data collection. Crystals diffracted

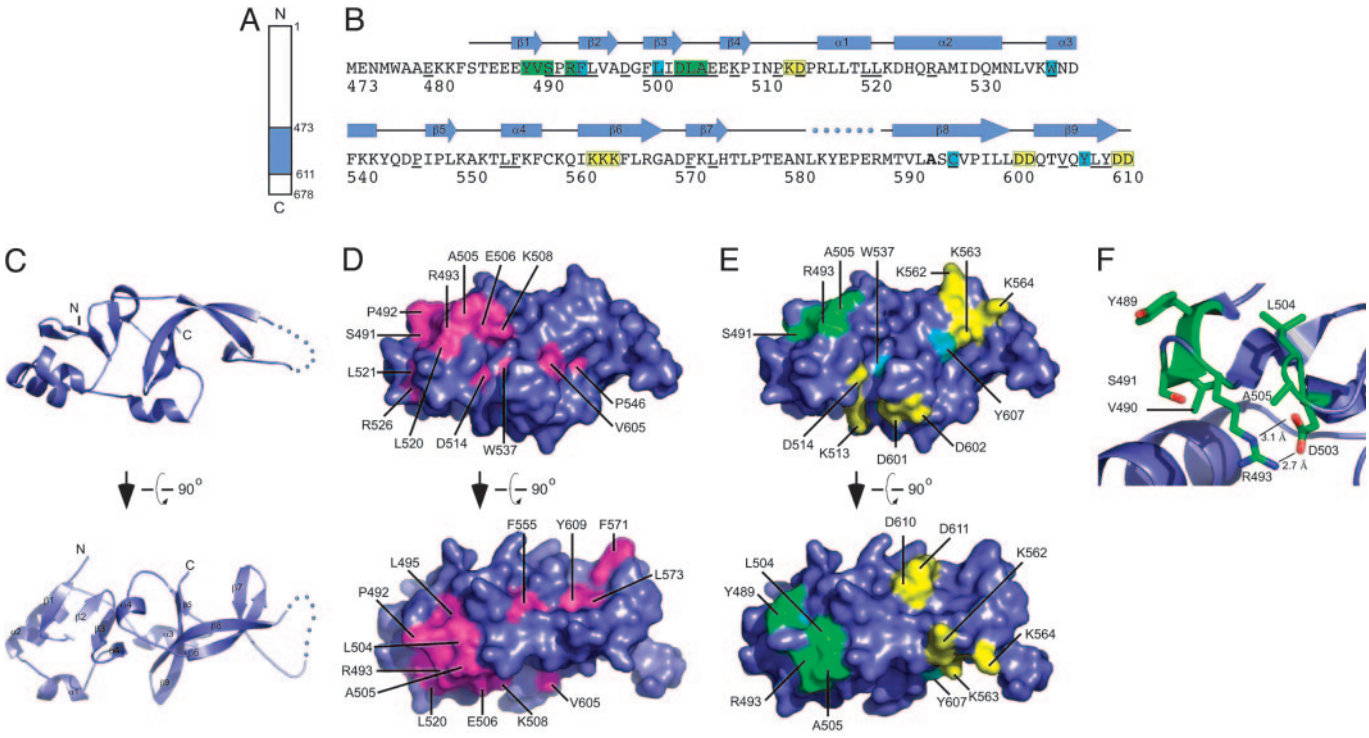

Fig. 1. Structure of the Sir1p-OIR. (*A*) Schematic diagram of *S. cerevisiae* Sir1p indicating the position of the Sir1p-OIR (residues 473–611) in blue. (*B*) Sequence, conservation, genetically determined roles, and secondary structure of Sir1p-OIR*. The Sir1p-OIR* sequence is colored to identify residues that are important for Orc1p binding (green), Sir4p binding (yellow), or binding for Orc1p and Sir4p (light blue). Sir1p residues that are invariant among the four yeast Sir1p homolog sequences are underlined. Residue 593, labeled in bold, is alanine in the described structure but is a cysteine in the natural *S. cerevisiae* Sir1p sequence. Secondary structural elements in the Sir1p-OIR* domain are shown above the sequence; the dotted line indicates a region where electron density was not observed. (*C*) Orthogonal views of a ribbon diagram of the crystal structure of Sir1p-OIR*. Secondary structure elements from *B* are labeled on the lower diagram. Ribbon diagrams and surface representations were rendered with PYMOL (26). (*D*) Orthogonal views of the surface conservation of Sir1p-OIR* with invariant residues (underlined in *B*) colored magenta and labeled. Views correspond to those in *C*. (*E*) Surface representation of Sir1p-OIR* colored as in *B* to indicate residues important for interaction with Orc1p, Sir4p, or both proteins (11). (*F*) Close-up view of previously identified Orc1p-interacting residues (ball-and-stick form) within the SRD module. Residues are labeled, and selected distances are indicated.

to 2.7-Å resolution with $P6_122$ symmetry and unit cell dimensions of $a = b = 72.15$ Å and $c = 310.89$ Å, consistent with one heterodimer per asymmetric unit (17).

Data were indexed and scaled by using HKL2000 (18), and the structure of the complex was determined by molecular replacement using AMORE (25) with the Orc1p-BAH (10) and Sir1p-OIR* domain structures as search models. The molecular replacement solution was refined with REFMAC5/ARP (23, 24) and by manually rebuilding the model with O (22).

Results and Discussion

Structure of the Sir1p-OIR. Direct physical interaction between Sir1p and ORC is critical for establishing silent chromatin at *HMR* and *HML* in *S. cerevisiae* (7, 10, 11). Previous studies identified the minimal OIR of Sir1p and amino acids within the OIR as important for the Sir1p/ORC interaction (8, 11) (Fig. 1 *A* and *B*). We carried out crystallization trials of the *S. cerevisiae* OIR in an effort to obtain the domain's high-resolution structure. These experiments were plagued with protein precipitation problems that were linked to intermolecular disulfide bonds formed between OIRs. Therefore, we considered the role of cysteine residues in the OIR. The domain contains three cysteine residues (C558, C593 and C595) that could be involved in disulfide bond formation (Fig. 1*B*). A comparison of the Sir1p-OIRs from *S. cerevisiae*, *Saccharomyces bayanus*, *Saccharomyces mikatae*, and *Saccharomyces castellii* indicated that C595 is invariant, consistent with the functional role for this cysteine in the *S. cerevisiae* OIR (11) (Fig. 1*B*). However, C558 and C593 are not conserved, indicating that these cysteine residues might be dispensable for OIR function. Analysis of individual mutant variants of the *S. cerevisiae* OIR indicated that a C593A substitution increased the solubility of the OIR and prevented disulfide bond-dependent heterogeneity (data not shown). Importantly, the mutant, OIR*, retained its interaction with the Orc1-BAH domain, and this interaction depended on Y489, a residue previously shown to be critical for the Sir1p/ORC interaction *in vivo* (*Supporting Materials and Methods* and Fig. 3, which are published as supporting information on the PNAS web site). Therefore, the C593A mutation that created OIR* did not disrupt the defined molecular function of the wild-type OIR, and OIR* was used for further structural analyses.

Crystals of selenomethionine-substituted OIR* were used to determine the structure of the domain to 2.5-Å resolution by using multiwavelength anomalous dispersion phasing methods (Table 1). The crystal form contained two molecules per asymmetric unit. The final model includes one molecule with residues 484–611, excluding residues 578–588 for which electron density was not observed, and a second molecule with residues 486–611, excluding residues 582–588. The excluded residues in both molecules lie in an exposed loop that connects two β-strands. The two OIR* molecules in the asymmetric unit superpose with a rms deviation of 0.378 Å for all 115 common C^{α} atoms, indicating that the molecules show no appreciable differences in fold.

OIR* forms a globular oval-shaped structure with dimensions of $50 \times 30 \times 15$ Å that is comprised of two apparent structural

BIOCHEMISTRY

subdomains (Fig. 1*C*). The first subdomain comprises the N-terminal half of OIR* and is formed by β-strands 1–4 and α-helices 1 and 2. This fold forms a four-stranded antiparallel β-sheet platform that is supported on one side by helices. The second C-terminal subdomain consists of the α3-helix and an elaborately intertwined core consisting of β-strands 5–9. OIR*'s two subdomains abut one another through an interface wherein a portion of the β-sheet from the N-terminal lobe is sandwiched between α4 and several loops connecting secondary structural elements from the C-terminal subdomain. Searches for proteins with structural similarity to the OIR* structure or its individual subdomains did not identify similar structures in the Protein Data Bank, indicating that the Sir1p-OIR is a previously uncharacterized fold.

Analysis of evolutionarily conserved surface features of OIR* indicates that there is a conserved region that is presented by the N-terminal subdomain β-sheet (Fig. 1*D*). As shown in Fig. 1*B*, only 29 of the 138 residues that comprise Sir1p-OIR are invariant across the four known yeast Sir1p sequences, with the vast majority mapping to the N-terminal subdomain. Although many of the conserved residues are buried in the domain's hydrophobic core, one surface comprised of conserved residues S491, P492, R493, L495, L504, A505, E506, K508, and L520 form a contiguous 570-Å^2 exposed area. These residues create a largely hydrophobic patch flanked by less conserved charged surface features (Fig. 4, which is published as supporting information on the PNAS web site). As described below, many of these residues have proven important for Sir1p's physical and functional interaction with Orc1p.

A Discrete Structural Module Within OIR* Contains Amino Acids Required for the Sir1p/ORC Interaction. In previous studies, we demonstrated that substitution of any one of seven amino acids (Y489, V490, S491, R493, D503, L504, or A505) within the silencer-recognition defective (SRD) region (defined as the region including these amino acids, i.e., Y489–A505) in the context of full-length Sir1p causes a SRD phenotype *in vivo*. The SRD phenotype is caused by a mutant Sir1p being unable to bind the silencer but able to establish silent chromatin if brought to the silencer by linkage to a heterologous DNA-binding domain (8, 9). We refer to mutant Sir1 proteins that cause the SRD phenotype as Sir1p^{srd}. Importantly, substitutions of SRD amino acids abolish a two-hybrid interaction between Sir1p and the Orc1-BAH domain but not between Sir1p and Sir4p, implying that they are properly folded (11). Based on these analyses, it was postulated that SRD amino acids were involved in direct contacts between Sir1p and ORC.

The OIR* structure shows that the SRD region (Y489–A505) forms a small discrete module within the N-terminal subdomain of OIR* and is comprised primarily of an antiparallel β-sheet (Fig. 1 *B* and *C*). Two small clusters of amino acids within this module were identified in our previous work as SRD residues. The first cluster includes residues from the β1-strand (Y489 and V490) and the loop connecting β-strands 1 and 2 (S491 and R493). The second comprises the C terminus of the β-strand 3 (D503) and the loop connecting β-strands 3 and 4 (L504 and A505). The two clusters come together to form a continuous surface on one face of the OIR* domain (Fig. 1*E*).

A detailed view of the SRD region shows that three of the SRD amino acid side chains are fully exposed to the surface and play no obvious role in the structural integrity of the OIR or the SRD module itself (Y489, L504, and A505) (Fig. 1*F*). S491 and R493 are each partially surface-exposed, but V490 is not exposed and appears to play a role in stabilizing interactions between β-strands 1 and 2. In addition, D503 forms electrostatic interactions with R493 that likely help stabilize the orientation and structure of the SRD module.

Substitutions of F494 or L501 abolish all defined functions of Sir1p (11). Thus, although these residues are located within the operationally defined SRD region (Y489–A505), neither F494 nor L501 are SRD residues. The OIR* structure shows that the side chains of both of these amino acids are buried in the core of the OIR and, therefore, like other buried amino acids, such as W537, C595, and Y607, contribute to the hydrophobic interactions that stabilize the folded OIR. A similar rationale could explain why mutations of most of the other residues in the SRD region that were not identified in the earlier genetic screen were not isolated. The exception is P492, which connects β-strands 1 and 2. The P492 side chain maps to the same surface location as the defined SRD amino acids (Fig. 1 *D* and *E*) and, as described below, plays a critical role in the interaction between OIR* and Orc1-BAH domain. It is possible that mutations of P492 were not isolated because of an important structural role of this residue in forming the turn between β-strands 1 and 2 and that alteration of this residue would result in defective Sir1p folding.

Residues Required for the Sir1p–Sir4p Two-Hybrid Interaction. Two-hybrid experiments indicate that, in addition to interacting with ORC, Sir1p interacts with Sir4p (7). A region of Sir1p sufficient for a Sir1p–Sir4p interaction extends from Sir1p I346 to the C terminus of Sir1p, D678 (11). The OIR, Y489–D611, is contained within the Sir4p-interaction region of Sir1p. Site-directed mutagenesis of clusters of charged residues identified three different clusters within the OIR portion of the Sir4p-interaction region required for a Sir1p/Sir4p interaction but dispensable for a Sir1p/ORC1p interaction (11). The OIR structure revealed that these clusters, K562–564A, D601–602A, and D610–611A, were exposed on three distinct surface patches on the OIR (Fig. 1 *B* and *E*). Thus, in contrast to the SRD amino acids required for a Sir1p/ORC1p interaction that formed one small patch on the surface of the OIR, amino acids required for a Sir1p/Sir4 interaction were scattered over four regions of the OIR that lie on three different faces of the globular domain (Fig. 1*E*). Further analysis of the Sir1p/Sir4p complex is necessary for a deeper understanding of how Sir1p and Sir4p interact, but these data provide evidence that electrostatic interactions could play a more significant role in Sir1p/Sir4p interactions than in Sir1p/ORC interactions.

Structure of the OIR*/Orc1p-BAH Domain Complex. To further define the structural basis for the Sir1p/ORC interaction, we crystallized and determined the 2.7-Å resolution structure of the Sir1p OIR* domain in complex with the Orc1p-BAH domain (OIR*/BAH) (Table 1). The crystal form contained one heterodimer per asymmetric unit. The final model includes residues 487–611 of Sir1p and 10–214 of Orc1p, excluding residues 27–36 of Orc1p for which very poor or no electron density was observed. The excluded residues of Orc1p are in a segment that was also absent from the isolated Orc1-BAH domain structure (10).

The OIR*/BAH complex is formed through an interaction that buries a surface area of 1,277 Å^2 (Fig. 2 *A* and *B*). The interaction surfaces of the two domains are highly complementary in terms of their shape and chemical composition. The BAH domain presents a concave surface comprised of residues from several regions of the protein domain. This surface has a highly hydrophobic center that is bordered by polar and charged residues. As described earlier, the OIR* interaction surface also presents a hydrophobic center with polar and charged residues toward its exterior (Fig. 4), which complements the BAH surface electrostatics. However, in contrast to the BAH interaction site, the OIR* interaction surface is convex in shape, which molds its interaction site into a form that fits neatly into the enveloping BAH domain. The structure of the isolated OIR* domain fragment superimposes

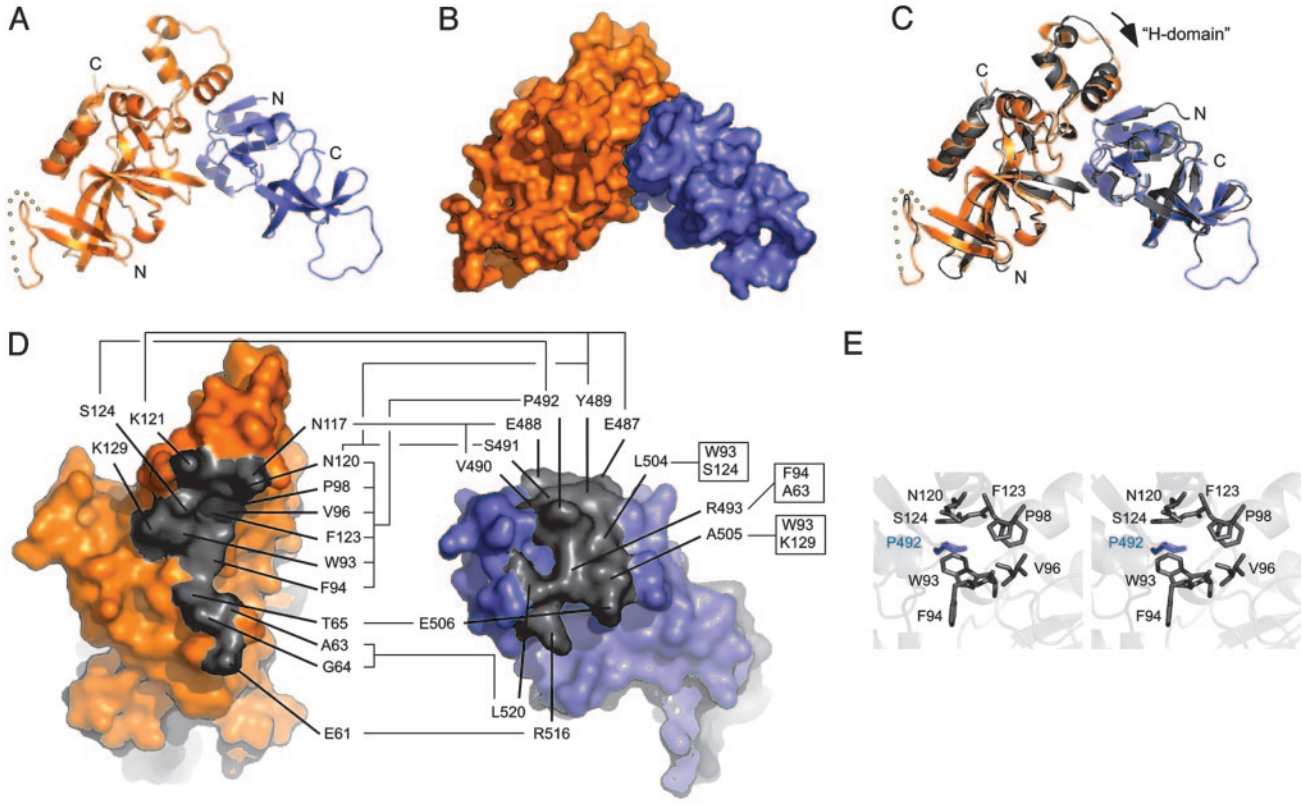

Fig. 2. Structure of the Sir1p-OIR*/Orc1p-BAH complex. (*A*) Ribbon diagram of the crystal structure of the Sir1p-OIR*/Orc1p-BAH complex, with Orc1p-BAH in orange and OIR* in blue. (*B*) Surface representation of structure shown in *A*. (*C*) Overlay of the complex structure from *A*, with the isolated Orc1p-BAH and Sir1 OIR structures shown in gray. The apparent movement of the H-domain of Orc1 is indicated by an arrow. (*D*) The two domains from the OIR*/BAH complex are rotated orthogonally and shown independently to expose the interacting surfaces on each domain. Residues that form the interface are colored gray and labeled. Specific residue contacts are indicated with connecting lines. (*E*) Stereoview P492 of OIR* in a binding pocket formed by several amino acids in the Orc1p-BAH domain.

onto the OIR* protomer in the OIR*/BAH complex with an rms deviation of 0.922 Å over all 114 common C^{α} atoms, implying that structural changes to the OIR* domain are quite minor upon binding the BAH domain (Fig. 2*C*). The BAH domain undergoes a more appreciable structural shift upon binding to the OIR, with an ≈3° rotation observed in a helical subdomain called the H-domain (Fig. 2*C*). This motion gives the BAH domain the subtle appearance of clamping down on the OIR.

Previous structural, biochemical, and genetic studies implicated the H-domain in Orc1p's interaction with Sir1p *in vitro* and silencing function *in vivo* (10). The H-domain consists of three small α-helices on a loop that is distinct from the conserved core of the BAH domain, which consists predominantly of a β-rich structure. The structure of the OIR*/BAH complex shows that the largest α-helix within the H-domain is indeed involved with direct contacts with the SRD region of the Sir1p OIR, as predicted (Fig. 2 *A*, *C*, and *D*). For example, Y489 on OIR* makes extensive contacts with K121 within BAH H-domain, consistent with the previous genetic analyses (8, 10, 11) and the strong *in vitro* interaction defect caused by a Y489A substitution in OIR* (*Supporting Materials and Methods* and Fig. 3). Other contacts between previously identified SRD amino acids and the H-domain of Orc1p are summarized in Fig. 2*D*.

In addition to the contacts between Sir1p and Orc1p implicated by experiments, the structure of the OIR*/Orc1p-BAH complex reveals previously uncharacterized contacts that appear important for the Sir1p/ORC interaction. In particular, as mentioned above, although P492 of Sir1p is surface-exposed and holds a prominent position with the SRD module of OIR*, previous genetic analyses failed to reveal P492 as important for Sir1p/ORC interactions (8). However, the structure of the OIR*/Orc1p-BAH complex reveals clearly that P492 of OIR* plays a prominent role in formation of the complex. Specifically, P492 of OIR* packs into a hydrophobic pocket formed by six residues on the Orc1p-BAH domain surface (Fig. 2 *D* and *E*). Three of the Orc1p amino acids that form this pocket (N120, F123, and S124) are from the H-domain, but the other three (W93, F94, and P98) are outside the H-domain in a loop linking a β-strand and an α-helix in Orc1p-BAH (10). As summarized in Fig. 2*D*, several additional contacts are made between the two protein domains that had not been previously identified (E506, R516, and L520 of Sir1p and E61, A63, G64, and T65 of Orc1p). Further investigation into the importance of these residues for the function of the Orc1/Sir1 complex will be required for a full accounting of their roles in the establishment of silent chromatin structures.

In summary, the structures of OIR* and the OIR*/BAH complex presented here elucidate the structural underpinnings of the previous and extensive genetic and molecular observations concerning the Sir1p/ORC interaction critical for the establishment of silent chromatin. In addition, new contributors to this important interaction are revealed by this study that should be useful in further analysis of how this interaction is regulated and controls silencing *in vivo*. It is interesting to note that, although the BAH domain is evolutionarily conserved, many of the amino acids within the Orc1p-BAH domain, including those within the

H-module that contact Sir1p, as illustrated by the structure presented in Fig. 2*C*, are not. This observation is consistent with the hypothesis that BAH domains perform dual functions: those associated with chromatin that require conserved structural elements within the BAH domain and specific roles that are tailored by evolution of unique protein–protein interaction motifs (10). If this hypothesis is correct, the structure of the Sir1p-SRD module may represent a yeast-specific mechanism for binding ORC that could serve as a foundation for the design of species-specific chemical modulators of ORC in fungal pathogens.

We thank Katrina Forest and Advanced Photon Source staff (Com-CAT and BioCARS beamlines) for help with data collection. This work was supported by National Institutes of Health Grant GM056890 (to C.A.F.) and Shaw Scientist Awards from the Milwaukee Foundation (to C.A.F. and J.L.K.). D.A.B. was supported in part by National Institutes of Health Training Grant in Molecular Biophysics GM08293.

1. Grewal, S. I. & Moazed, D. (2003) *Science* **301,** 798–802.
2. Weinreich, M., Palacios DeBeer, M. A. & Fox, C. A. (2004) *Biochim. Biophys. Acta* **1677,** 142–157.
3. Fischle, W., Wang, Y. & Allis, C. D. (2003) *Curr. Opin. Cell Biol.* **15,** 172–183.
4. Rusche, L. N., Kirchmaier, A. L. & Rine, J. (2003) *Annu. Rev. Biochem.* **72,** 481–516.
5. Bell, S. P. (2002) *Genes Dev.* **16,** 659–672.
6. Chien, C. T., Buck, S., Sternglanz, R. & Shore, D. (1993) *Cell* **75,** 531–541.
7. Triolo, T. & Sternglanz, R. (1996) *Nature* **381,** 251–253.
8. Gardner, K. A., Rine, J. & Fox, C. A. (1999) *Genetics* **151,** 31–44.
9. Gardner, K. A. & Fox, C. A. (2001) *Genes Dev.* **15,** 147–157.
10. Zhang, Z., Hayashi, M. K., Merkel, O., Stillman, B. & Xu, R. M. (2002) *EMBO J.* **21,** 4600–4611.
11. Bose, M. E., McConnell, K. H., Gardner-Aukema, K. A., Muller, U., Weinreich, M., Keck, J. L. & Fox, C. A. (2004) *Mol. Cell. Biol.* **24,** 774–786.
12. Fox, C. A. & McConnell, K. H. (2005) *J. Biol. Chem.* **280,** 8629–8632.
13. Bell, S. P., Mitchell, J., Leber, J., Kobayashi, R. & Stillman, B. (1995) *Cell* **83,** 563–568.
14. Gavin, K. A., Hidaka, M. & Stillman, B. (1995) *Science* **270,** 1667–1671.
15. Callebaut, I., Courvalin, J. C. & Mornon, J. P. (1999) *FEBS Lett.* **446,** 189–193.
16. Goodwin, G. H. & Nicolas, R. H. (2001) *Gene* **268,** 1–7.
17. Matthews, B. W. (1968) *J. Mol. Biol.* **33,** 491–497.
18. Otwinowski, Z. & Minor, W. (1997) in *Methods in Enzymology*, eds. Carter, C. W. & Sweet, R. M. (Academic, New York), Vol. 276A, pp. 307–26.
19. Terwilliger, T. C. & Berendzen, J. (1999) *Acta Crystallogr. D* **55**, 849–861.
20. Otwinowski, Z. (1991) *Proc. CCP4 Study Weekend*, eds. Wolf, W., Evans, P. R. & Leslie, A. G. W. (Daresbury Laboratory, Warrington, U.K.), pp. 80–86.
21. Cowtan, K. (1994) *Joint CCP4 ESF-EACBM Newsletter on Protein Crystallography* (Daresbury Laboratory, Warrington, U.K.), Vol. 31, p. 34.
22. Jones, T. A., Zou, J. Y., Cowan, S. W. & Kjeldgaard, M. (1991) *Acta Crystallogr. A* **47,** 110–119.
23. Winn, M. D., Isupov, M. N. & Murshudov, G. N. (2001) *Acta Crystallogr. D* **57,** 122–133.
24. Lamzin, V. S. & Wilson, K. S. (1993) *Acta Crystallogr. D* **49,** 129–147.
25. Navaza, J. (2001) *Acta Crystallogr. D* **57,** 1367–1372.
26. Delano, W. L. (2002) PYMOL: A Molecular Graphics System (DeLano Scientific, San Carlos, CA).